

# NLS Bifurcations on the bowtie combinatorial graph and the dumbbell metric graph

Roy H. Goodman

September 6, 2018

## Abstract

We consider the bifurcations of standing wave solutions to the nonlinear Schrödinger equation (NLS) posed on a quantum graph consisting of two rings connected by a single edge, the so-called dumbbell, recently studied in [17]. The authors of that study found the ground state undergoes two bifurcations, first a symmetry-breaking, and the second which they call a symmetry preserving bifurcation. We clarify the type of the symmetric-preserving bifurcation and show that it is transcritical. We then reduce the question, and show that the phenomena described in that paper can be reproduced in a simple discrete self-trapping equation on a combinatorial graph of bowtie shape. This allows for complete analysis both by geometric methods and by parameterizing the full solution space. We then expand the question, and describe the bifurcations of *all* the standing waves of this system, which can be classified into three families, and of which there exists a countably infinite set.

## 1 Introduction

Linear and nonlinear waves on quantum graphs have recently gained a lot of attention in mathematical literature as a nontrivial generalization of well-known systems and because they possess novel mathematical properties not possible in simpler geometry [3, 4]. In physics they may arise in optical systems, Bose-Einstein condensates, and in the study of large molecules such as carbon nanotubes [5, 7, 16, 19]. In the nonlinear regime they lead to bifurcations and to interesting questions about the existence of minimizers [6, 21, 22].

While there is an infinite variety of graphs, a lot of recent work has gone into a few simple ones. The tadpole graph consists of a half-line joined to a ring at a single vertex [20]. The lollipop graph is similar, with the half-line replaced by a finite line segment [3]. Star graphs consist of a finite number of half lines or line segments that meet at a single vertex [1].

In a recent paper, Marzuola and Pelinovsky study the bifurcations of stationary solutions to the cubic nonlinear Schrödinger equation posed on a dumbbell-shaped quantum graph [17], in which two rings are connected via a line segment. At small  $L^2$  norm, the ground state, i.e. the lowest energy solution with that norm, is constant in the spatial coordinate. They show that this state undergoes two bifurcations as the solution amplitude is increased. The first is a symmetry-breaking or pitchfork bifurcation and the second they call a “symmetry preserving” bifurcation, producing a solution localized on the central edge of the graph. At the symmetry-breaking solution, the asymmetric solution becomes the ground state, and for sufficiently large amplitude, the non-constant solution that arises from the second bifurcation becomes the ground state.

We show that all of these phenomena are present in a simpler system, a discrete NLS equation on a graph with five vertices. We show that in this simpler system the “symmetry preserving” bifurcation is actually a transcritical bifurcation, and, thus, contains a branch of solutions not present in the bifurcation diagram shown in [17]. We then show, via a perturbation calculation, and via numerical calculations that the same is true for the problem on the quantum graph, which demonstrates the existence of the branch not found in [17]. Further, we show that the nonlinear problem possesses a much larger set of stationary solutions.

## 1.1 NLS on combinatorial and metric graphs

The focusing cubic nonlinear Schrödinger equation (NLS)

$$i\partial_t\Psi = \Delta\Psi + |\Psi|^2\Psi, \quad (1.1)$$

subject to appropriate boundary conditions or conditions at infinity, is perhaps the most-studied system in nonlinear waves, arising as an envelope equation in systems where dispersion is roughly balanced by nonlinearity. It is the simplest PDE with both these features, and thus is widely used as a model problem. Many variants of this equation have been studied in order to explore a wide range of phenomena.

One of the simplest is the discrete nonlinear Schrödinger equation (DNLS) in which the spatial derivative is replaced by a discrete second difference operator

$$i\dot{u}_n + u_{n-1} - 2u_n + u_{n+1} + |u_n|^2 u_n = 0. \quad (1.2)$$

If the total number of sites is small this system is also known as the discrete self trapping (DST) system, which has a long history [11, 12, 14].

NLS may be generalized to graphs in a number of ways. Before doing so, we first set notation, briefly summarizing that of Berkolaiko [3]. Let  $\Gamma = (\mathcal{V}, \mathcal{E})$  be a combinatorial graph, i.e. a finite collection of vertices  $\mathcal{V} = \{\mathbf{v}_n, n = 1, \dots, N\}$  connected pairwise by a collection of edges  $\mathcal{E} = \{\mathbf{e}_m = (\mathbf{v}_i, \mathbf{v}_j), m = 1, \dots, M\}$ . The graph is called *directed* if  $(\mathbf{v}_i, \mathbf{v}_j)$  is distinguished from  $(\mathbf{v}_j, \mathbf{v}_i)$ . Otherwise it is *undirected*.

If  $\Gamma$  has no self-directed edges, i.e. no edges of the form  $(\mathbf{v}_i, \mathbf{v}_i)$ , the incidence matrix is defined to be the  $N \times M$  matrix  $E$  in which

$$E_{nm} = \begin{cases} 1 & \text{if edge } m \text{ points to vertex } n, \\ -1 & \text{if edge } m \text{ points from vertex } n, \\ 0 & \text{otherwise.} \end{cases}$$

Let there be a positive weight  $w_m$  associated to edge  $\mathbf{e}_m$  and let  $W$  be a diagonal matrix with  $W_{mm} = w_m$ . If unstated, then  $W$  is assumed to be the identity matrix. Then the (weighted) Laplacian

$$L_\Gamma = EWE^\top$$

is a positive definite matrix, and the DST equation now reads

$$i\dot{\mathbf{u}} = L_\Gamma\mathbf{u} + \mathcal{N}(\mathbf{u}), \quad (1.3)$$

where  $\mathcal{N}(\mathbf{u})_j = |u_j|^2 u_j$ . While a directed graph is necessary for forming  $E$  and thus  $L_\Gamma$ , the matrix  $L_\Gamma$  is unchanged if the direction of any edge is interchanged.

A *metric graph* is a directed graph in which a length  $\ell_m$  has been assigned to each edge  $\mathbf{e}_m$ , as well as a coordinate  $x_m$  with  $0 < x_m < \ell_m$  which increases in the specified direction of the edge. A function  $f(x)$  defined on the graph is simply a collection of functions  $f_m(x_m)$  defined on the individual edges  $\mathbf{e}_m$  such that  $f(x)|_{\mathbf{e}_m} = f_m(x_m)$ . A Schrödinger operator  $\mathcal{L}_\Gamma$  defined on such functions,

$$\mathcal{L}_\Gamma|_{\mathbf{e}_m} = -\partial_{x_m}^2 + V_m(x_m) \quad (1.4a)$$

and which requires a boundary condition at the vertices, defines a *quantum graph*. This allows us to extend the definition of equation (1.1) to metric graphs. We will set the potential along each edge to  $V_m(x_m) = 0$ . The most common is the Kirchhoff boundary condition, which states that the solution is continuous at the vertices, i.e. letting  $\Psi|_{\mathbf{e}_m} = \psi_m$ ,

$$\psi_{m_1}(\mathbf{v}_n) = \psi_{m_2}(\mathbf{v}_n), \quad \forall m_1, m_2 \in \mathcal{V}_n, \quad (1.4b)$$

where  $\mathcal{V}_n$  is the set of all edges incident on vertex  $\mathbf{v}_n$ , and further, that the total flux through any vertex is zero, i.e

$$\sum_{m \in \mathcal{V}_n} (-1)^{\sigma_m} \partial_{x_m} \psi_m(\mathbf{v}_n) = 0, \quad (1.4c)$$

where  $\sigma_m = 0$  if  $\mathbf{v}_n$  is the initial point on edge  $\mathbf{e}_m$  and  $\sigma_m = 1$  if it is the final point. Both ends of an edge that connects a single vertex to itself contribute to this sum.

## 1.2 Previous work on the dumbbell quantum graph

Ref. [17] considers standing wave solutions to the NLS equation of the form  $\Psi(x, t) = \Phi(x)e^{i\Lambda t}$ , which solve

$$\mathcal{L}_\Gamma \Phi - 2|\Phi|^2 \Phi = \Lambda \Phi, \quad (1.5)$$

on a dumbbell-shaped graph with two vertices and three edges, as displayed in Figure 1.1. Two of this graph's edges are rings connecting the two vertices to themselves, and the third connects them. It makes the symmetry assumption  $\ell_1 = \ell_3$  which, without loss of generality they take to be  $\ell_1 = \ell_3 = 2\pi$ , and let  $\ell_2 = 2L$ , parameterized by  $-\pi < x_{1,3} < \pi$  and  $-L < x_2 < L$ .

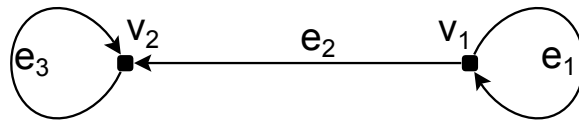


Figure 1.1: The dumbbell graph with its vertices and edges labeled.

We note that symmetries of the graph play a role in the solutions to a quantum graph NLS system. The underlying dumbbell metric graph has the following three reflection symmetries, which we state somewhat informally:

$$\mathcal{R}_1 : \text{Reverse the direction of edge } \mathbf{e}_1. \quad (1.6a)$$

$$\mathcal{R}_2 : \text{Exchange the labels of edges } \mathbf{e}_1 \text{ and } \mathbf{e}_3 \text{ and of vertices } \mathbf{v}_1 \text{ and } \mathbf{v}_2 \text{ and reverse the direction of edge } \mathbf{e}_2. \quad (1.6b)$$

$$\mathcal{R}_3 : \text{Reverse the direction of edge } \mathbf{e}_2. \quad (1.6c)$$

A first step is to enumerate all the eigenfunctions and eigenvalues on the dumbbell obtained by ignoring the nonlinear term in Equation (1.5),

$$\mathcal{L}_\Gamma \Phi = \lambda \Phi. \quad (1.7)$$

On each edge, the eigenfunction satisfies  $\phi_m''(x_m) + \lambda \phi_m(x_m) = 0$ , and thus the restriction of each eigenfunction to a single edge is simply a sine or cosine function, and the eigenfunctions are obtained by enforcing the boundary conditions (1.4b) and (1.4c).

This observation is made systematic using the secular determinant, which is well-described by Berkolaiko [3]. The nonzero eigenvalues are of the form  $\lambda = k^2$  where  $k$  solves

$$\Sigma(k) = \det M(k) = \det (I - SD(k)) = 0, \quad (1.8)$$

and the dimension of the square matrices  $S$  and  $D(k)$  is twice the number of edges. This equation is derived by assuming that the solution is given as a linear combination of  $e^{ikx_j}$  and  $e^{-ikx_j}$  on each edge  $\mathbf{e}_j$ , and enforcing that the vertex conditions be satisfied. For the dumbbell graph,

$$S = \frac{1}{3} \begin{pmatrix} 2 & -1 & 0 & 2 & 0 & 0 \\ -1 & 2 & 0 & 2 & 0 & 0 \\ 2 & 2 & 0 & -1 & 0 & 0 \\ 0 & 0 & -1 & 0 & 2 & 2 \\ 0 & 0 & 2 & 0 & 2 & -1 \\ 0 & 0 & 2 & 0 & -1 & 2 \end{pmatrix} \text{ and } D(k) = \begin{pmatrix} e^{ik\epsilon} & 0 & 0 & 0 & 0 & 0 \\ 0 & e^{ik\epsilon} & 0 & 0 & 0 & 0 \\ 0 & 0 & e^{ik\pi} & 0 & 0 & 0 \\ 0 & 0 & 0 & e^{ik\pi} & 0 & 0 \\ 0 & 0 & 0 & 0 & e^{ik\epsilon} & 0 \\ 0 & 0 & 0 & 0 & 0 & e^{ik\epsilon} \end{pmatrix}.$$

After some manipulations, equation (1.8) is equivalent to

$$(\sin k(L - \pi) - 3 \sin k(L + \pi)) (\cos k(L - \pi) - 3 \cos k(L + \pi)) (\sin^2 k\pi) = 0. \quad (1.9)$$

The three factors of equation (1.9) correspond to three families of eigenfunctions:

**Even Eigenfunctions** Solutions in this family are nonzero on all three edges and satisfy  $\mathcal{R}_2(\Phi) = \Phi$ . The eigenvalues in this family are labeled as  $\omega_j^2$ ,  $j = 0, 1, \dots$  in [17]. The linear ground state  $\Phi_0 = 1$  is a member of this family, although the secular determinant equation holds only for  $k \neq 0$ .

**Odd Eigenfunctions** Solutions in this family are nonzero on all three edges and satisfy  $\mathcal{R}_2(\Phi) = -\Phi$ . The eigenvalues in this family are labeled as  $\Omega_j^2$ ,  $j = 1, 2, \dots$  in [17].

**Ring-centered Eigenfunctions** Solutions in this family have multiplicity two and can be normalized such that their support lies entirely on one or the other of the edges  $\mathbf{e}_1$  and  $\mathbf{e}_3$  and satisfy  $\mathcal{R}_1(\Phi) = -\Phi$  and  $\mathcal{R}_3(\Phi) = -\Phi$ . These solutions are given by  $\Phi(x) = \sin(kx_m)$ ,  $k = 1, 2, \dots$  on the edge  $\mathbf{e}_m$  where they are supported and have eigenvalues  $k^2$ .

If  $L$  is chosen as an integer multiple of  $\pi/2$ , eigenvalues from the rings may coincide with those of the even and odd eigenfunctions. We will assume no such resonances exist. Numerical examples, computed using the finite element discretization of Arioli [2], are shown in figure 1.2.

Ref. [17] then considers the continuations of these standing waves into the nonlinear regime, where

$$Q(\Phi) = \sum_{m=1}^M \int_{\mathbf{e}_m} |\phi_m(x_m)|^2 dx_m, \quad (1.10)$$

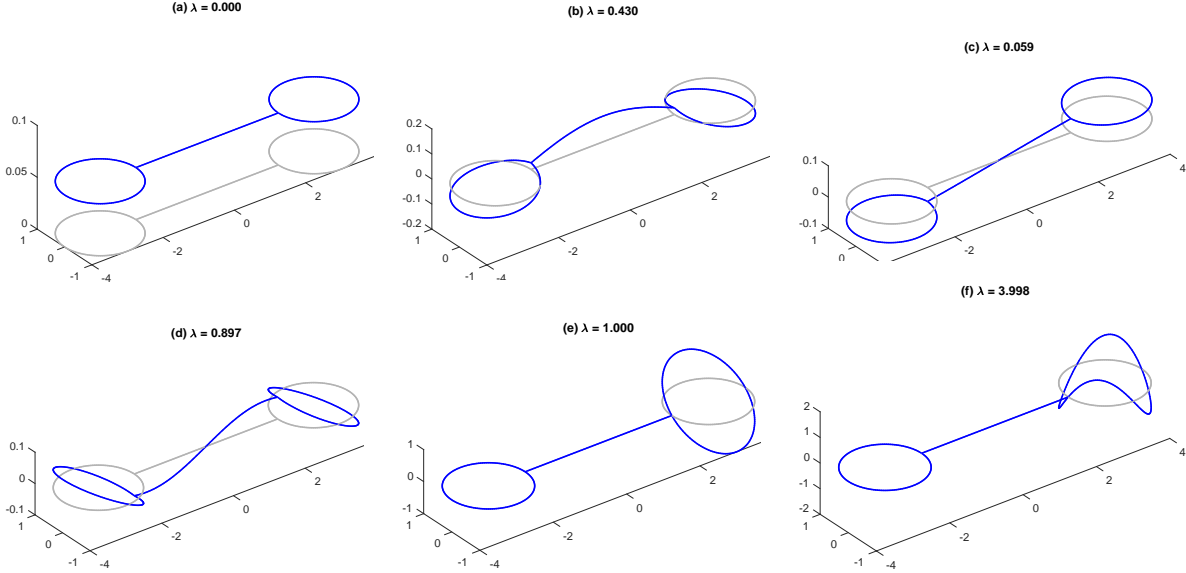


Figure 1.2: The first two members of the even family of eigenfunctions (a-b), odd family (c-d), and ring-centered family (e-f) of the linear eigenvalue problem (1.7) on the dumbbell graph, computed numerically, along with the associated eigenvalues. In subfigure (f) the analytical value is obviously  $\lambda = 4$ , giving an indication of the accuracy of this computation.

the squared  $L^2$  norm of the solution, can be used as a bifurcation parameter, and where the linear problem applies in the limit of vanishing norm. The restriction of a standing wave to an individual edge can here be determined in terms of Jacobi elliptic functions; see Appendix A.

Ref. [17] shows that the constant solution  $\Phi_0$  undergoes a pair of bifurcations with increasing  $Q$ , equivalently with decreasing  $\Lambda$ . The first is a symmetry-breaking bifurcation, at which the newly-created states are not invariant to  $\mathcal{R}_2$  but which together form a group orbit for that symmetry. More concretely, two nonlinear eigenfunctions  $\Phi_{\text{left}}$  and  $\Phi_{\text{right}}$  emerge, each asymmetric, but with  $\Phi_{\text{left}} = \mathcal{R}_2(\Phi_{\text{right}})$ . The second, which they call a “symmetry-preserving” bifurcation, gives rise to a symmetric solution that is concentrated along the central edge  $\mathbf{e}_2$  of the dumbbell as  $\Lambda \rightarrow -\infty$ . It also proves that for sufficiently large values of  $|\Lambda|$  and for all  $L > 0$ , the symmetric solution has smaller  $Q$  than the asymmetric solution, becoming the nonlinear ground state.

A bifurcation diagram computed in Ref. [17] for  $L = \pi/2$  is shown in Figure 1.3, showing the two bifurcations discussed in that paper. The present paper was initially motivated by two questions: to understand what exactly occurs at the symmetry preserving bifurcation and to determine whether this effect is novel to the dumbbell quantum graph or if, instead, it occurs in simpler systems. The answers are simple: the symmetry-preserving bifurcation is of transcritical type, and the same phenomenon can be found in a significantly simpler system, the bowtie combinatorial graph. It appears that the closed rings in both the dumbbell and the bowtie contribute to the transcritical nature of the second bifurcation. In a simpler related problem, the Schrödinger equation on an interval with Neumann boundary conditions, all the bifurcations are pitchforks. This distinction is due to a subtle breaking of symmetry by the rings, as we shall discuss. Moreover, on the lollipop graph, featuring one ring and one straight edge, all of these bifurcations are transcritical.

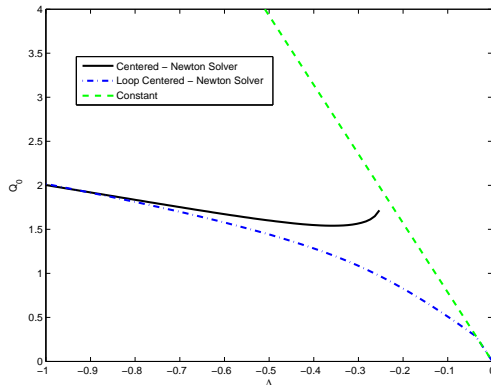


Figure 1.3: A numerically computed bifurcation diagram from Ref. [17].

### 1.3 Organization

The remainder is organized as follows. Section 2 introduces a simple combinatorial graph model that reproduces the two bifurcations seen in [17] for the dumbbell quantum graph. Section 3 describes arguments using perturbation theory and numerical continuation that show that the symmetry preserving bifurcation is indeed transcritical and to recover the half-branch of solutions not discussed in [17]. Section 4 describes a singular limit of the dumbbell graph in which the length of edges  $e_1$  and  $e_3$  approaches zero. This demonstrates what is so interesting about the ring-shaped edges. Section 5 contains a full classification and enumeration of all types of standing waves possible on the dumbbell graph. This is based on the observation that there are two types of behavior possible at the two vertices, and therefore three types of standing waves, as the two vertices can both have the first behavior, both have the second, or be different. After making this classification, we use a combination of exact solution formulae and numerical continuation to draw bifurcation diagrams for the three types of solutions. In fact, each of the three families are countably infinite. Section 6 wraps up and discusses some possible future directions.

## 2 Three approaches to the bowtie combinatorial graph

Here we introduce a simpler combinatorial graph which undergoes the same sequence of bifurcations described in the previous section, consisting of five vertices, joined into a bowtie configuration as in Figure 2.1.

Setting the weights to one, the Laplacian matrix is

$$L_{\Gamma} = \begin{pmatrix} 2 & -1 & -1 & 0 & 0 \\ -1 & 2 & -1 & 0 & 0 \\ -1 & -1 & 4 & -1 & -1 \\ 0 & 0 & -1 & 2 & -1 \\ 0 & 0 & -1 & -1 & 2 \end{pmatrix}, \quad (2.1)$$

with eigenvalues  $\lambda_1 = 0$ ,  $\lambda_2 = 5$ ,  $\lambda_3 = 1$ , and  $\lambda_4 = \lambda_5 = 3$  (numbered in this strange order

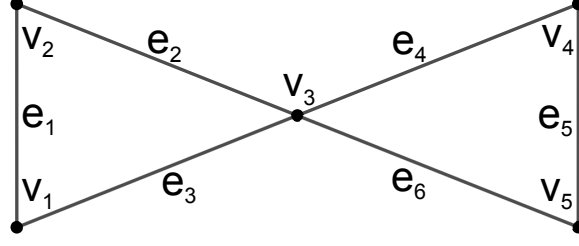


Figure 2.1: The bowtie combinatorial graph.

purposely) and associated normalized eigenvectors,

$$\mathbf{v}_1 = \frac{1}{\sqrt{5}} \begin{pmatrix} 1 \\ 1 \\ 1 \\ 1 \\ 1 \end{pmatrix}, \mathbf{v}_2 = \frac{1}{\sqrt{20}} \begin{pmatrix} 1 \\ 1 \\ -4 \\ 1 \\ 1 \end{pmatrix}, \mathbf{v}_3 = \frac{1}{2} \begin{pmatrix} -1 \\ -1 \\ 0 \\ 1 \\ 1 \end{pmatrix}, \mathbf{v}_4 = \frac{1}{\sqrt{2}} \begin{pmatrix} 1 \\ -1 \\ 0 \\ 0 \\ 0 \end{pmatrix}, \mathbf{v}_5 = \frac{1}{\sqrt{2}} \begin{pmatrix} 0 \\ 0 \\ 0 \\ 1 \\ -1 \end{pmatrix}.$$

The DST system on this graph is invariant to left multiplication by the three permutations, in cyclic notation,

$$R_1 = (12), R_2 = (14)(25), \text{ and } R_3 = (45),$$

which are discrete analogs of the symmetries (1.6). The space  $\mathcal{S}_1 = \text{span}\{\mathbf{v}_1, \mathbf{v}_2\}$  is invariant under  $R_1, R_2,$  and  $R_3$ , while the space  $\mathcal{S}_2 = \text{span}\{\mathbf{v}_1, \mathbf{v}_2, \mathbf{v}_3\}$  is invariant under just  $R_1$  and  $R_3$ . The space  $\mathcal{S}_3 = \text{span}\{\mathbf{v}_4, \mathbf{v}_5\}$  is invariant under  $R_2$ . Put more simply, on  $\mathcal{S}_1$ ,  $u_1 = u_2 = u_4 = u_5$ , on  $\mathcal{S}_2$ ,  $u_1 = u_2$  and  $u_4 = u_5$ , and on  $\mathcal{S}_3$ ,  $u_1 = -u_2$ ,  $u_3 = 0$ , and  $u_4 = -u_5$ .

The Hamiltonian for the DST is

$$H = \bar{\mathbf{u}}^\top L_\Gamma \mathbf{u} - \frac{1}{2} \sum_{j=1}^5 |u_j|^4. \quad (2.2)$$

The change of variables to diagonalize the linear part,

$$\mathbf{u} = \sum_{j=1}^5 z_j \mathbf{v}_j,$$

is canonical and results in the Hamiltonian

$$\begin{aligned} H = & 5|z_2|^2 + |z_3|^2 - 3|z_4|^2 - 3|z_5|^2 - \frac{1}{50}|z_1 - 2z_2|^4 \\ & - \frac{1}{800} \left( \left| 2z_1 + z_2 + \sqrt{5}z_3 + \sqrt{10}z_4 \right|^4 + \left| 2z_1 + z_2 + \sqrt{5}z_3 - \sqrt{10}z_4 \right|^4 \right. \\ & \left. + \left| 2z_1 + z_2 - \sqrt{5}z_3 + \sqrt{10}z_5 \right|^4 + \left| 2z_1 + z_2 - \sqrt{5}z_3 - \sqrt{10}z_5 \right|^4 \right). \end{aligned} \quad (2.3)$$

In these coordinates, the subspaces  $\mathcal{S}_1$ – $\mathcal{S}_3$  are all invariant under the dynamics of  $H$ , which are now written as  $\mathcal{S}_1 = \{(z_1, z_2, 0, 0, 0)\}$ ,  $\mathcal{S}_2 = \{(z_1, z_2, z_3, 0, 0)\}$ ,  $\mathcal{S}_3 = \{(0, 0, 0, z_4, z_5)\}$ .

## 2.1 Linear Stability via Symmetry Reduction on $\mathcal{S}_2$

The two bifurcations discussed in Ref. [17] take place on the invariant subspace  $\mathcal{S}_2$ , obtained by setting  $z_4 = z_5 = 0$  in Hamiltonian (2.3). The symplectic change of variables

$$z_1 = \sqrt{R - |y_2|^2 - |y_3|^2} e^{i\phi}, \quad z_2 = y_2 e^{i\phi}, \quad z_3 = y_3 e^{i\phi}$$

yields a Hamiltonian that is independent of  $\phi$ , thus its conjugate variable  $R = |z_1|^2 + |z_2|^2 + |z_3|^2$  is conserved. This reduces the number of degrees of freedom to two. In these variables, the continuation of the linear ground state is represented by  $y_2 = y_3 = 0$ . The leading order quadratic part of the Hamiltonian is given by

$$H = 5|y_2|^2 + |y_3|^2 - \frac{R}{10} \left( y_2^2 + 2|y_2|^2 + \bar{y}_2^2 \right) - \frac{R}{10} \left( y_3^2 + 2|y_3|^2 + \bar{y}_3^2 \right).$$

This yields linearized evolution equations

$$i\dot{y}_2 = 5y_2 - \frac{R}{5} (y_2 + \bar{y}_2), \quad i\dot{y}_3 = y_3 - \frac{R}{5} (y_3 + \bar{y}_3),$$

with eigenvalues

$$\lambda = \pm \sqrt{\frac{2R}{5} - 1} \text{ and } \lambda = \pm \sqrt{2R - 25}.$$

For small values of  $R$  all eigenvalues are imaginary and the ground state is stable. The system has bifurcations at  $R = \frac{5}{2}$  and  $R = \frac{25}{2}$ , which we will see are of pitchfork and transcritical type, respectively, and involve the directions  $y_3$  and  $y_2$ , respectively.

## 2.2 Geometric Reduction

In order to better understand the analog of ‘‘symmetry preserving’’ bifurcation of Ref. [17], we consider the restriction to the invariant subspace  $\mathcal{S}_1$  on which solutions are invariant to all three discrete symmetries. On this subspace

$$H = 5|z_2|^2 - \frac{1}{10}|z_1|^4 - \frac{1}{10} \left( z_1^2 \bar{z}_2^2 + 4|z_1|^2 |z_2|^2 + \bar{z}_1^2 z_2^2 \right) + \frac{3}{10} |z_2|^2 (z_1 \bar{z}_2 + \bar{z}_1 z_2) - \frac{13}{40} |z_2|^4. \quad (2.4)$$

This Hamiltonian is  $S^1$  invariant, i.e.  $H(e^{i\phi} z_1, e^{i\phi} z_2) = H(z_1, z_2)$ . This implies that  $|z_1|^2 + |z_2|^2$  is conserved, i.e. that trajectories are confined to three-spheres. Therefore the following change of coordinates, the Hopf fibration of  $S^3$ , which is standard in geometric mechanics [13], applies. Let

$$R = |z_1|^2 + |z_2|^2, \quad Z = |z_1|^2 - |z_2|^2, \quad X + iY = 2\bar{z}_1 z_2. \quad (2.5)$$

Then a simple calculation confirms that

$$R^2 = X^2 + Y^2 + Z^2 \quad (2.6)$$

is conserved and is in fact a Casimir for the reduced system and that  $(X, Y, Z)$  evolve under the non-canonical Hamiltonian equations

$$\frac{d}{dt} \begin{pmatrix} X \\ Y \\ Z \end{pmatrix} = -\nabla \frac{R^2}{2} \times H(X, Y, Z),$$

where in these coordinates

$$H = -\frac{5Z}{2} + \frac{3RX}{20} + \frac{9RZ}{80} - \frac{X^2}{20} - \frac{3XZ}{20} + \frac{Y^2}{20} - \frac{Z^2}{160} + \left( \frac{5R}{2} - \frac{33R^2}{160} \right).$$

Then  $(X, Y, Z)$  evolve according to

$$\dot{X} = \frac{1}{80}(-9R + 12X + 9Z + 200)Y; \quad (2.7a)$$

$$\dot{Y} = \frac{1}{80}(-12X^2 + 7XZ + 12Z^2 + (9R - 200)X - 12RZ); \quad (2.7b)$$

$$\dot{Z} = \frac{1}{20}(3R - 4X - 3Z)Y. \quad (2.7c)$$

The fixed points then satisfy  $Y = 0$  (which implies that  $z_1/z_2 \in \mathbb{R}$ ) and, from equations (2.6) and (2.7b)

$$X^2 + Z^2 = R^2; \quad (2.8a)$$

$$-12X^2 + 7XZ + 12Z^2 + (9R - 200)X - 12RZ = 0. \quad (2.8b)$$

These are the equations for a circle and a hyperbola. The solution  $(X, Z) = (0, R)$  holds for all positive values of  $R$  and retracing our steps, corresponds to the continuation of the linear ground state solution  $\mathbf{u} \propto \mathbf{v}_1$ .

For small values of  $R$  there are two fixed points. The second corresponds to the linear solution  $\mathbf{u} \propto \mathbf{v}_2$  which approaches  $(X, Z) \approx (0, -R)$  as  $R \rightarrow 0^+$ . As  $R$  increases there are two bifurcations. First at  $R \approx 7.57$ ,<sup>1</sup> the other branch of the hyperbola crosses the circle, leading to a new pair of fixed points. At  $R = 8$ , the branches of the hyperbola merge and re-connect, which is not itself a bifurcation of fixed points, but sets the stage for a transcritical bifurcation at  $R = \frac{25}{2}$ . This is the analog of Marzuola's "symmetry-preserving bifurcation;" see Figure 2.2.

### 2.3 Parameterization of solution branches

Another illustration of the transcritical nature of the bifurcation can be seen in a remarkable parameterization of the symmetric standing-wave solutions to the reduced system with Hamiltonian (2.4), based on a parameterization from [12]. We look for stationary solutions of the form

$$z_1 = ae^{i\Omega t}, \quad z_2 = be^{i\Omega t}; \quad a, b, \Omega \in \mathbb{R}.$$

These satisfy the nonlinear system

$$a - b - a^3 - \Omega a = 0; \quad (2.9a)$$

$$-4a + 4b - b^3 - \Omega b = 0. \quad (2.9b)$$

Subtracting the two and factoring yields

$$(a - b)(a^2 + ab + b^2 + \Omega - 5) = 0.$$

---

<sup>1</sup>The precise value, computed by eliminating  $Z$  from system (2.8) using the resultant, and then setting the discriminant with respect to  $X$  to zero is  $R = -13 - \sqrt{241 - 12 \cdot 15^{2/3}} + \sqrt{482 + 12 \cdot 15^{2/3} + \frac{7378}{\sqrt{241 - 12 \cdot 15^{2/3}}}}$ .

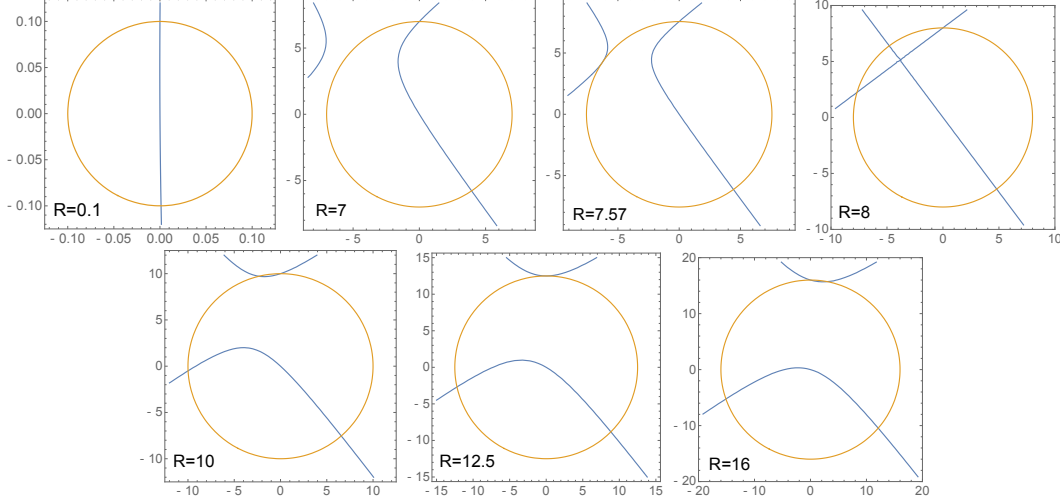


Figure 2.2: The solutions of system (2.8) in  $(X, Z)$ , given by the intersections of the two curves, showing the sequence of bifurcations described in the text. Note in particular that for  $R = 10$  there exists a fixed point just to the left of  $(0, R)$ , which has moved to the right for  $R = 16$ .

Thus system (2.9) has one family of constant-valued solutions  $b = a$ ,  $\Omega = -a^2$ . These are just the nonlinear continuation of the ground state. To construct the other solution, make the ansatz

$$\begin{aligned} a &= A\sqrt{5 - \Omega} \sin(\theta - \alpha); \\ b &= A\sqrt{5 - \Omega} \sin(\theta + \alpha). \end{aligned}$$

Here we look for a one-parameter family indexed by  $\theta$ , and seek solutions for  $\alpha$  and  $A$ , which satisfy

$$A^2 (4 \sin^2 \alpha - 3) \sin^2 \theta - A^2 \sin^2 \alpha + 1 = 0,$$

which can be solved by letting  $\alpha = \frac{\pi}{3}$  and  $A = \frac{2}{\sqrt{3}}$ . Plugging this into the equations, solving for  $\Omega$  and simplifying yields

$$\begin{aligned} a &= -\sqrt{2} \cos\left(\theta + \frac{\pi}{6}\right) \sqrt{\csc 3\theta (3\sqrt{3} \cos \theta - 5 \sin \theta)} \\ b &= \sqrt{2} \cos\left(\theta - \frac{\pi}{6}\right) \sqrt{\csc 3\theta (3\sqrt{3} \cos \theta - 5 \sin \theta)} \\ \Omega &= 5 - \frac{3}{2} \csc 3\theta (3\sqrt{3} \cos \theta - 5 \sin \theta). \end{aligned}$$

At  $\theta = \frac{\pi}{2}$ , this yields  $a = b = \sqrt{-\Omega} = \sqrt{\frac{5}{2}}$ , agreeing with the constant solution. Thus, these two branches cross in a transcritical bifurcation. This parameterization yields three distinct branches: for  $0 < \theta < \frac{\pi}{3}$ , for  $\frac{\pi}{3} < \theta < \frac{2\pi}{3}$ , and for  $\frac{2\pi}{3} < \theta < \pi$ . However for  $\tan^{-1}\left(\frac{3\sqrt{3}}{5}\right) < \theta < \frac{\pi}{6}$  and  $\frac{2\pi}{3} < \theta < \pi$ , this formula yields  $4a^2 + b^2 < 0$ , a strange result that can be interpreted to yield solutions to the differential equation with the sign of the nonlinearity reversed. The branch with  $0 < \theta < \tan^{-1}\frac{3\sqrt{3}}{5}$  corresponds to the nonlinear continuation of the eigenvector  $\mathbf{v}_2$ . The relevant branch for the transcritical bifurcation corresponds to  $\frac{\pi}{3} < \theta < \frac{2\pi}{3}$ .

The same idea can be applied to find the branch arising due to the pitchfork bifurcation at  $\Omega = -\frac{1}{2}$ . In this case, we let  $u_1 = u_2 = a$ ,  $u_3 = b$ , and  $u_4 = u_5 = c$ , so the reduced system has three equations

$$a - b - a^3 - \Omega a = 0; \quad (2.10a)$$

$$-2a + 4b - 2c - b^3 - \Omega b = 0; \quad (2.10b)$$

$$-b + c - c^3 - \Omega c = 0. \quad (2.10c)$$

Subtracting the first equation from the third yields

$$(c - a)(a^2 + ac + c^2 + \Omega - 1) = 0.$$

We look for solutions that set the second factor to zero using the ansatz

$$a = A\sqrt{1 - \Omega} \sin(\theta - \alpha), \quad c = A\sqrt{1 - \Omega} \sin(\theta + \alpha)$$

and find again that  $A = \frac{2}{\sqrt{3}}$ , and  $\alpha = \frac{\pi}{3}$ . Substituting these values back into equation (2.10a) or (2.10c) yields

$$a = \frac{2}{\sqrt{3}}\sqrt{1 - \Omega} \sin\left(\theta - \frac{\pi}{6}\right), \quad b = \frac{-2(1 - \Omega)^{3/2} \sin(3\theta)}{3\sqrt{3}}, \quad c = \frac{2}{\sqrt{3}}\sqrt{1 - \Omega} \sin\left(\theta + \frac{\pi}{6}\right).$$

Finally, plugging this into equation (2.10b) yields a quartic equation for  $\Omega$  with coefficients depending on  $\sin^2 \theta$ . This quartic equation factors into linear and cubic terms. The linear factor yields the branch that bifurcates from  $\Omega = 1$ , i.e. from the linear eigenfunction  $\mathbf{v}_3$ . The branch that concerns us corresponds to the real root obtained by setting the cubic factor to zero using Cardano's formula, and applies on the interval  $\frac{\pi}{3} < \theta < \frac{2\pi}{3}$ . As both the cubic factor and its solution by Cardano's formula yield complicated and un-illuminating formulas, we choose not to include them. However we note that that

$$\lim_{\theta \rightarrow \frac{\pi}{3}^+} (a, b, c) = (0, 0, \infty), \quad \lim_{\theta \rightarrow \frac{2\pi}{3}^-} (a, b, c) = (\infty, 0, 0), \quad \text{and } (a, b, c)|_{\theta=\frac{\pi}{2}} = \frac{(1, 1, 1)}{\sqrt{2}},$$

displaying the expected symmetry and bifurcating, as it should from a pitchfork bifurcation.

Figure 2.3 shows the bifurcation of the branches just discussed. In particular, it shows that the constant state is the ground state from the linear limit  $\Omega \rightarrow 0$  until it bifurcates in the pitchfork bifurcation at  $\Omega = -\frac{1}{2}$ . The constant solution undergoes a transcritical bifurcation at  $\Omega = -\frac{5}{2}$ , creating two branches of symmetric solutions, one concentrated at the center point  $u_3$ , which initially extends to the right from the bifurcation point, before turning around at a bifurcation at  $\Omega \approx -1.94$  (this value is the root of a quartic polynomial), and becomes the ground state when it appears to cross the branch of asymmetric solutions in this figure at  $\Omega \approx -2.97$ . This crossover is a principal finding of Ref. [17]. Note that the tangency between the two branches is the signature of the transcritical bifurcation in a power/frequency plot, as discussed by Yang [23]. As this branch heads left from the bifurcation with constant solution, it approaches a family of symmetric solutions where  $u_3 \rightarrow 0$  and the value at the other four locations becomes large as  $\Omega \rightarrow -\infty$ . In fact we find that the asymmetric branch satisfies  $R \sim 2 - 2\Omega$  and the symmetric branch satisfies  $R \sim 4 - \Omega$  as  $\Omega \rightarrow -\infty$ , confirming that the symmetric branch is the ground state for large negative  $\Omega$ .

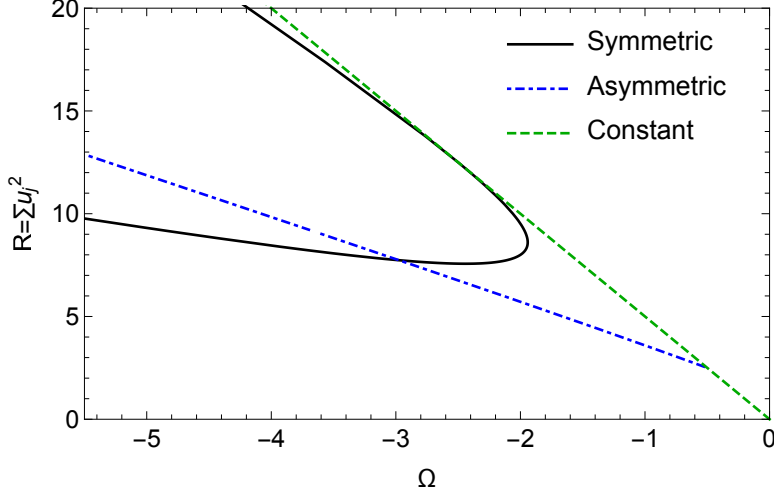


Figure 2.3: Bifurcations of the constant solution to the bowtie-shaped DST system.

### 3 The symmetry-preserving bifurcation in the dumbbell graph

We now return to the dumbbell quantum graph. Its restriction to the edges solves the double-well oscillator equation (1.5), whose phase plane is shown in Figure 3.1, with trajectories lying along level sets of the energy

$$E = \frac{1}{2} (\Phi'^2 + \Lambda \Phi^2 + \Phi^4). \quad (3.1)$$

For all  $\Lambda$ ,  $\Phi = 0$  is an exact solution, and for  $\Lambda < 0$ , there are additional fixed points at

$$\Phi = \pm \sqrt{-\Lambda/2}. \quad (3.2)$$

These nonzero fixed points correspond to constant-valued solutions to system (1.4). Except for the separatrix solutions for  $\Lambda < 0$ , all orbits of equation (1.5) are periodic. Exact formulas are provided in A1

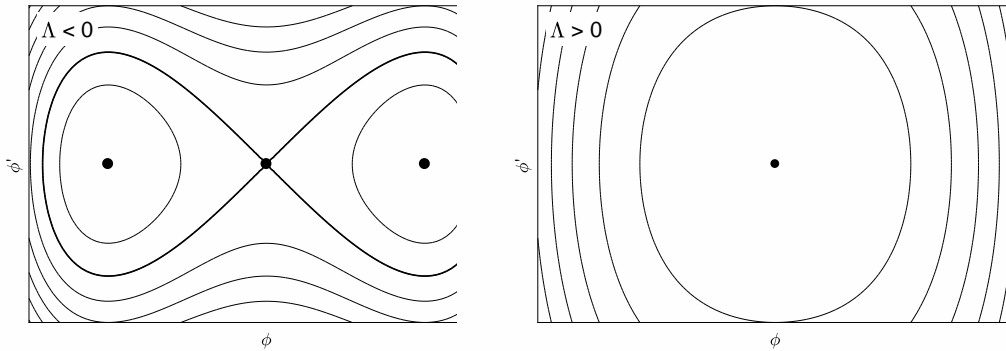


Figure 3.1: The phase plane of Equation (1.5), whose trajectories are level sets of the energy given by Equation (3.1).

### 3.1 Numerical continuation study

Ref. [17] finds that the constant-valued solution (3.2) to system (1.4) undergoes two bifurcations as  $\Lambda$  is decreased from zero. We numerically compute both branches using pseudo-arclength continuation. We use centered differences to discretize system (1.5), and second-order one-sided differences to discretize the vertex condition (1.4c) on the dumbbell-shaped graph depicted in Figure 1.1. The system is solved using Newton’s method, combined with pseudo-arclength continuation as described in the textbook of Nayfeh and Balachandran [18]. The result of a computation with  $L = 2$  is shown in Figure 3.2. It captures the branch not present in Figure 1.3 and is remarkably similar to Figure 2.3. Two solutions from this branch with frequency  $\Lambda \approx -2$  are shown in Figure 3.3.

The completed branch arises in a saddle node bifurcation at  $\Lambda \approx -0.192$  and then crosses the branch of constant-valued solutions in a transcritical bifurcation near  $\Lambda = -\omega_1^2 \approx -0.215$ , in exactly the same manner that we found for DST on the bowtie graph. Note that here it is more convenient to think of  $\Lambda$  as the bifurcation parameter, since  $Q$  does not appear explicitly in the equation for stationary solutions.

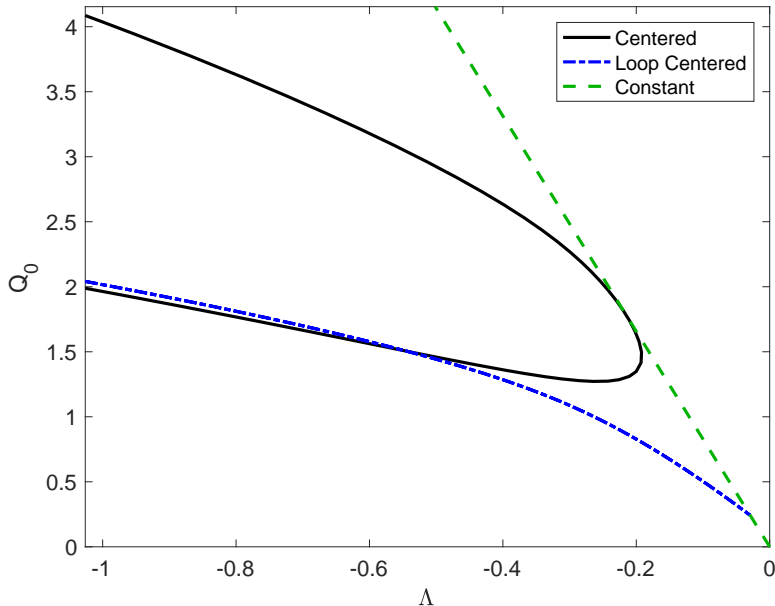


Figure 3.2: Numerical continuation of the PDE on the quantum graph revealing the existence of the transcritical bifurcation.

### 3.2 Perturbation Analysis

Ref. [17] contains a perturbation theory parameterizing symmetry-broken solutions close to the constant-valued solution using, essentially, the Poincaré-Lindstedt method. It also contains a remark that a similar expansion is possible for the second bifurcation, but, as classifying this bifurcation is not the focus of that paper, the authors elect not to carry it out. We briefly review their solution, and present in more detail the expansion showing that the second bifurcation is transcritical.

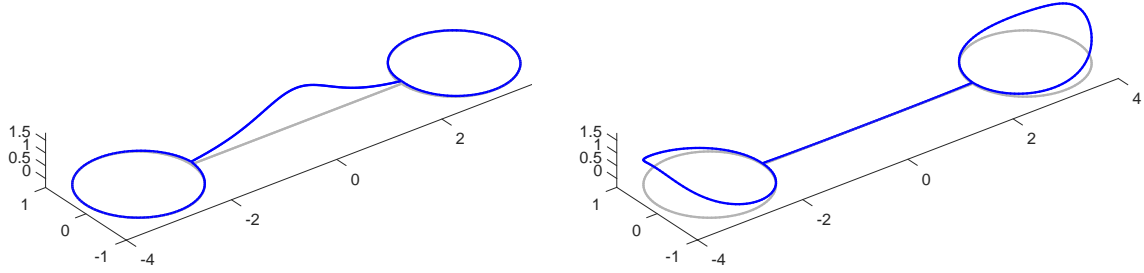


Figure 3.3: (Left) Large-amplitude solution on the half-branch discovered in Ref. [17]. (Right) Large-amplitude two-soliton solution.

### 3.2.1 The Pitchfork Bifurcation

Recalling that  $\Omega_1^2$  is the eigenvalue belonging to the first member of the second family of eigenpairs, the constant solution (3.2) becomes unstable at  $(\Lambda, \Phi) = (-\Omega_1^2/2, \Omega_1/2)$  [17, Lemma 3.2]. Let  $\Phi_{\text{odd}}$  be the odd-symmetric eigenfunction corresponding to the eigenvalue  $\Omega_1^2$ , normalized such that  $\int_{\Gamma} \Phi_{\text{odd}}^2 dx = 1$ . Then the perturbation solution is given by

$$\begin{aligned}\Phi &= \frac{\Omega_1}{2} + a\Phi_{\text{odd}} + a^2\Phi_2 + a^3\Phi_3 + O(a^4); \\ \Lambda &= \frac{-\Omega_1^2}{2} + a^2\beta_2 + a^3\beta_3 + O(a^4).\end{aligned}$$

In order to solve for terms at  $O(a^2)$ , we must satisfy a Fredholm condition at  $O(a^3)$  but we do not otherwise need the terms at that higher order.

We find

$$\beta_2 = 9\Omega_1^2 \int_{\Gamma} \Phi_{\text{odd}}^2 \tilde{\Phi}_2 dx \quad \text{and} \quad \Phi_2 = \tilde{\Phi}_2 - \frac{\beta_2}{2\Omega_1},$$

where  $\tilde{\Phi}_2$  is the unique even-symmetric solution to

$$-(\Delta + \Omega_1^2)\tilde{\Phi}_2 = \Phi_{\text{odd}}^2.$$

This is well-defined since the null space of the self-adjoint operator on the left is spanned by the odd-symmetric function  $\Phi_{\text{odd}}$  and the right-hand side has even symmetry. Ref. [17] notes that this equation may be solved explicitly, and uses the exact solution to prove the direction in which the solution branch bends.

### 3.2.2 The Transcritical Bifurcation

Recalling that  $\omega_1^2$  is the eigenvalue belonging to the first member of the first family of eigenpairs, the constant solution bifurcates the second time at  $(\Lambda, \Phi) = (-\omega_1^2/2, \omega_1/2)$  [17, Remark 3.5]. Let  $\Phi_{\text{even}}$  be the even-symmetric eigenfunction corresponding to the eigenvalue  $\omega_1^2$ , normalized such that  $\int_{\Gamma} \Phi_{\text{even}}^2 dx = 1$ . Then the perturbation solution is given by

$$\begin{aligned}\Phi &= \frac{\omega_1}{2} + a\Phi_1 + a^2\Phi_2 + a^3\Phi_3 + O(a^4); \\ \Lambda &= \frac{-\omega_1^2}{2} + a\beta_1 + a^2\beta_2 + a^3\beta_3 + O(a^4).\end{aligned}$$

This differs from the previous expansion in the constant term needed in the  $\Phi$  expansion at  $O(a)$  and from the presence in the  $\Lambda$  expansion of an  $O(a)$  term. This leads a sequence of equations:

$$\begin{aligned} O(a) : \quad & -(\Delta + \omega_1^2) \Phi_1 = \frac{\omega_1 \beta_1}{2}; \\ O(a^2) : \quad & -(\Delta + \omega_1^2) \Phi_2 = \frac{\omega_1 \beta_2}{2} + \beta_1 \Phi_1 + 3\omega_1 \Phi_1^2; \\ O(a^3) : \quad & -(\Delta + \omega_1^2) \Phi_3 = \frac{\omega_1 \beta_3}{2} + \beta_2 \Phi_1 + \beta_1 \Phi_2 + 6\omega_1 \Phi_1 \Phi_2 + 2\Phi_1^3. \end{aligned}$$

At  $O(a)$  we find that  $\Phi_1 = \Phi_{\text{even}} + C$  and  $\beta_1 = -2\omega_1 C$ , with  $C$  to be determined. The equation at  $O(a^2)$  then becomes

$$-(\Delta + \omega_1^2) \Phi_2 = \omega_1 \left( \frac{\beta_2}{2} + C^2 \right) + \omega_1 (4C\Phi_{\text{even}} + 3\Phi_{\text{even}}^2).$$

The constant term is solvable, but the remaining term must be orthogonal to  $\Phi_{\text{even}}$  for solvability. This then yields a condition

$$C = -\frac{3}{4} \int_{\Gamma} \Phi_{\text{even}}^3 dx. \quad (3.3)$$

Solving the equation at this order yields

$$\Phi_2 = -\frac{1}{\omega_1} \left( \frac{\beta_2}{2} + C^2 \right) + \tilde{\Phi}_2,$$

where  $\tilde{\Phi}_2$  is the unique solution to

$$\begin{aligned} -(\Delta + \omega_1^2) \Phi_2 &= \omega_1 (4C\Phi_{\text{even}} + 3\Phi_{\text{even}}^2); \\ \int_{\Gamma} \tilde{\Phi}_2 \Phi_{\text{even}} dx &= 0. \end{aligned}$$

A Fredholm condition at  $O(a^3)$  then yields

$$\beta_2 = -4C^2 + \int_{\Gamma} \Phi_{\text{even}}^4 dx + \frac{3\omega_1}{2} \int_{\Gamma} \tilde{\Phi}_2 \Phi_{\text{even}}^2 dx.$$

This bifurcation must be transcritical because the expansion for  $\Lambda$  contains a term of  $O(a)$ , which was absent for the pitchfork bifurcation. This means that, letting  $\Lambda$  serve as bifurcation parameter, the “new” branch of solutions is present on both sides of the bifurcation. In addition, the profiles of the two new solutions that arise in the pitchfork bifurcation are “mirror images” of each other, because of the parity of  $\Phi_{\text{odd}}$ , or, more formally, they form a group orbit under the action of  $\mathcal{R}_2$ . There is no such symmetry between the two new solutions on opposite sides of the bifurcation point in the transcritical case.

We remark further that the expansions described in this section are equally valid for every eigenvalue/eigenfunction pair in the even or odd families. Thus, the constant-valued solution undergoes a pitchfork bifurcation each time its value crosses a frequency  $-\omega_j^2/2$  and a transcritical bifurcation each time it crosses a frequency  $-\Omega_j^2/2$ . We delay discussion of the bifurcations that involve the ring-centered families of eigenfunctions to Section 5.

## 4 Comparison with simpler quantum graphs

We were able to gain some insight into the dumbbell graph by considering the simpler problem of the bowtie combinatorial graph. Here we consider two additional simpler problems, the cubic Schrödinger problem defined on an interval with Neumann boundary conditions, and the problem on the lollipop graph, obtained from the graph in Figure 1.1 by removing the edge  $\mathbf{e}_3$  and imposing a Neumann condition at vertex  $\mathbf{v}_2$ .

The former can be thought of as a quantum graph consisting of just one edge and two vertices. This system, which can be derived as a singular limit of the dumbbell graph, has a different bifurcation structure. In what follows, we rescale the  $x$  coordinates along the edges of the dumbbell graph so that  $\ell_1 = \ell_3 = \epsilon$  and  $\ell_2 = \pi$ . The secular determinant equation (1.9) becomes:

$$\left( \sin \frac{k(\pi - \epsilon)}{2} - 3 \sin \frac{k(\epsilon + \pi)}{2} \right) \left( \cos \frac{k(\pi - \epsilon)}{2} - 3 \cos \frac{k(\epsilon + \pi)}{2} \right) \left( \sin^2 \frac{k\epsilon}{2} \right) = 0$$

The solutions to these the three factors correspond, respectively in the order presented, to the even, odd, and ring-centered families of eigenfunctions. For the ring-centered families, this gives  $k = 2n\pi/\epsilon$ , a sort of boundary layer. For the other two branches we may expand the wavenumber  $k = \sum_{j=0}^{\infty} \epsilon^j k_j$ . For the even-symmetric solutions we find  $k_0 = 2n$  and for the odd-symmetric,  $k_0 = 2n - 1$  and in both cases

$$k = k_0 \left( 1 - \frac{2\epsilon}{\pi} + \frac{4\epsilon^2}{\pi^2} \right) + \epsilon^3 \frac{\pi^2 k_0^3 - 16k_0}{2\pi^3} + O(\epsilon^4).$$

Letting the parameterization on the edge  $\mathbf{e}_2$  be given by  $0 < x_2 < \pi$ , then all the eigenfunctions are of the form  $\cos kx$  with  $k \approx 2n$  on the even family and  $k \approx (2n - 1)$  on the odd family.

Now, we take the singular limit  $\epsilon \rightarrow 0^+$ . The boundary layer solutions disappear, and the problem on the central edge  $\mathbf{e}_2$  reduces to the Schrödinger equation on an interval with Neumann conditions, whose eigenfunctions are simply  $\cos nx$ . We examine the sequence of bifurcations undergone by the nonlinear standing wave with constant spatial profile  $\Phi$  and frequency  $\Lambda = -2\Phi^2$  for this system. This solution undergoes a sequence of bifurcations at the discrete sequence of frequencies  $\Lambda_n = -n^2/2$ . Each of these bifurcations is a pitchfork, independently of the parity of  $n$  and in contrast to the dumbbell system, which alternates between pitchfork and transcritical bifurcations.

The difference between the problem on the interval and that on the dumbbell is that the Neumann problem on the interval has an additional symmetry: namely, the solution on the interval can be extended to the whole real line under an even periodic extension. Consider a solution in a neighborhood of the pitchfork bifurcation. In both the Neumann problem and the dumbbell problem, the solution looks to leading order like  $\Phi = \text{constant} + a\Phi_{\text{odd}}$ . Reversing the sign of  $a$  is equivalent to applying the symmetry  $\mathcal{R}_2$  to this solution. This argument fails near the transcritical bifurcation on the dumbbell: reversing the sign of  $a$  is not equivalent to applying a symmetry. However, in the limit  $\epsilon = 0$ , a new symmetry appears, as the evenly extended eigenfunctions have an odd symmetry about each of their zeros. This symmetry persists for nonlinear standing waves.

It is not necessary that there be rings appended to the interval. In the family of graphs pictured in Figure 4.1, the extra symmetry of the Neumann interval is also destroyed, and pitchforks involving even eigenfunctions will also be converted to transcriticals.

Therefore, we can expect that as  $\epsilon \searrow 0$ , each of the transcritical bifurcations on the dumbbell graph becomes increasingly pitchfork-like. While this statement should hold in a neighborhood

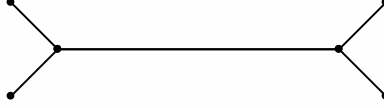


Figure 4.1: A graph that should have similar bifurcations.

of the bifurcations, for large values of  $|\Lambda|$ , the two branches will contain, respectively, one or two pulses, and thus diverge. We investigate this possibility by re-computing the continuation calculation shown in Figure 3.2 for large values of  $L$  in Figure 4.2, which correspond to small values of  $\epsilon$ . These show the width of the branch narrows greatly for large  $L$ , and appears more like a pitchfork.

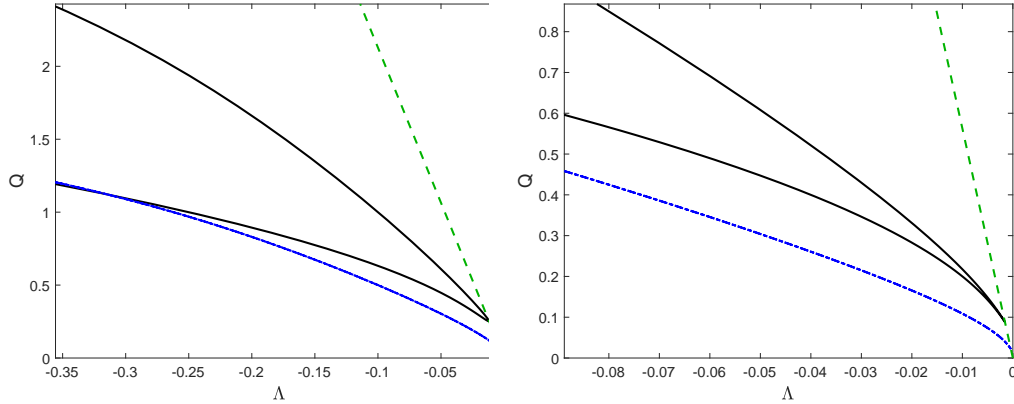


Figure 4.2: The analogy of figure 3.2 with  $L = 15$  and  $L = 50$ . As  $L$  is increased, the angle with which the two branches of solution approach the transcritical bifurcation decreases, making it appear, locally, more like a pitchfork.

Finally, we note that in the lollipop graph, lacking the symmetry of the dumbbell, the analysis leading to the pitchfork bifurcation in Section 3.2.1 is not applicable, but that the analysis in Section 3.2.2 would go through without any changes. Therefore we see that eliminating both rings leads to only pitchforks, while eliminating only one leads to only transcriticals. This is an answer to what is special about the dumbbell structure that allows both behaviors. The bifurcation diagram for the lollipop graph will become important in Section 5.4 when we discuss standing waves on the dumbbell that are built from lollipop standing waves.

## 5 Complete enumeration of stationary solutions

Given the attention that we have just paid to just two bifurcations, we should point out that the behavior of standing waves is significantly more complex. We have already pointed out that the constant-valued solution undergoes an alternating sequence of pitchfork and transcritical bifurcations, each time its frequency crosses  $\Lambda = -\Omega_j^2/2$  or  $\Lambda = -\omega_j^2/2$ . In addition, each of the other linear eigenfunctions can be continued into the nonlinear regime in a similar manner. In the remainder of this section, we will numerate all possible branches of stationary solutions using a combination of numerical continuation, phase planes, and analytical reasoning. A similar enumeration of standing waves was carried out for the tadpole graph by Noja et al. [20].

## 5.1 Two types of rings

We may classify the different types of stationary solutions by their behavior on the self-connected edge  $\mathbf{e}_1$  (or equivalently  $\mathbf{e}_3$ ). Since the solution along edge  $\mathbf{e}_1$  lies along a level set of the energy, continuity condition (1.4b) requires  $\phi_1(-\pi) = \phi_1(\pi)$  and thus, by the symmetry of the phase planes across the  $y$ -axis in Figure 3.1

$$\phi_1'(\pi) = \pm\phi_1'(-\pi). \quad (5.1)$$

Thus there are two cases. If Equation (5.1) is satisfied with a minus sign, then condition (1.4c) implies that  $\phi_2'(-L) = 2\phi_1'(\pi)$ . We will call such a ring *incomplete*. Note that when  $L$  is not a multiple of  $\pi/2$  both rings of eigenfunctions from the even and odd families are of this type; compare Figure 1.2(a-d). A simple calculation demonstrates that if  $\mathbf{e}_2$  is a complete ring, then  $E(\mathbf{e}_1) < E(\mathbf{e}_2)$ .

If Equation (5.1) is satisfied with the plus sign, then  $\phi_2'(-L) = 0$  and the solution on the self-directed edge must consist of an integer number of periods of a closed orbit. We will call such a ring *complete*. The nonzero ring of ring-centered eigenfunctions are of this type; see Figure 1.2(e-f). Note that self-directed edges on which the solution is identically zero satisfy can be considered both complete and incomplete. In contrast with incomplete rings, if  $\mathbf{e}_2$  is an complete ring, then  $E(\mathbf{e}_1) > E(\mathbf{e}_2)$ .

Therefore, there are three possible types of stationary solution. On the first, both rings are incomplete. On the second, both rings are incomplete, and the third contain one complete and one incomplete ring.

## 5.2 Two incomplete rings

We can search for these stationary solutions with two complete rings using the following shooting argument. All such stationary solutions must satisfy  $\frac{d\phi_j}{dx_j}\Big|_{x_j=0}$ ,  $j = 1, 3$ . Now define  $f(q, \Lambda, L) = \phi_3'(0)$  found by solving the following three consecutive initial value problems for equation (1.5):

1. Solve for  $\phi_1(x)$  from  $x_1 = 0$  to  $x_1 = \pi$  with initial condition  $\phi_1(0) = q$ ,  $\phi_1'(0) = 0$ .
2. Solve for  $\phi_2(x)$  from  $x_2 = -L$  to  $x_2 = L$  with initial condition  $\phi_2(-L) = \phi_1(\pi)$ ,  $\phi_2'(-L) = 2\phi_1'(\pi)$ .
3. Solve for  $\phi_3(x)$  from  $x_3 = -\pi$  to  $x_3 = 0$  with initial condition  $\phi_3(-\pi) = \phi_2(L)$ ,  $\phi_3'(-\pi) = \frac{1}{2}\phi_2'(L)$ .

Then solutions of  $f(q, \Lambda, L) = 0$  correspond to solutions of (1.5) on  $\Gamma$  with the appropriate vertex conditions. This definition is closely related to the map defined by Pelinovsky and Schneider over one cell of an infinite periodic graph [22]. We may then continue these solutions as a function of  $\Lambda$  to follow the branches and find bifurcations.

To follow this procedure, we first fix  $\Lambda = -1$  and  $L = 2$  and compute  $f(q, \Lambda, L)$  over an appropriate interval, which is shown in Figure 5.1. By standard arguments about continuous dependence on initial conditions,  $f$  is a continuous function of  $q$  and we can guarantee finding all such solutions by resolving this graph adequately. We then use MATCONT, a MATLAB continuation package, to trace these branches, varying  $\Lambda$  and holding  $L$  fixed [8, 9]. This is summarized in an incomplete but complex bifurcation diagram in Figure 5.2, which follows all the solutions to  $f(q, -1, 2) = 0$  with  $0 < q < 1.3$ .

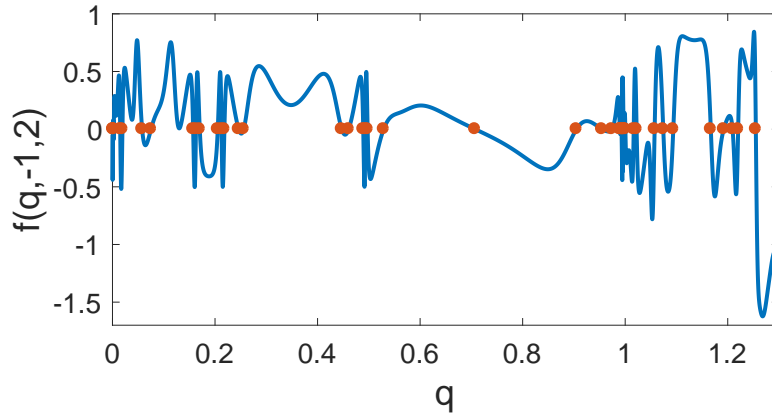


Figure 5.1: The shooting function described in the text whose zeros correspond to nonlinear standing waves on the graph  $\Gamma$ .

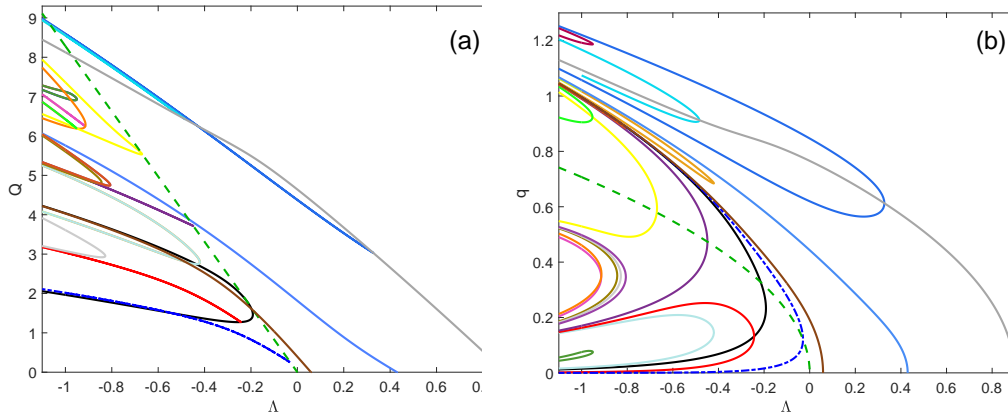


Figure 5.2: Two views of a partial bifurcation diagram with  $L = 2$ . (a) Plotting  $Q$  the squared  $L^2$  norm of the standing wave solutions. (b) Plotting the value  $q$  used in the shooting function. Colors of branches are consistent between the two panels and with Figure 3.2.

First, we find the previously mentioned branches arising alternately in pitchfork and transcritical bifurcations from the constant state. We also note that all other even-symmetric branches undergo symmetry breaking as well, e.g. near  $\Lambda = -0.2$  there is a red curve emanating from a black curve. This black curve is the centered branch found in Ref. [17], which becomes the ground state for large  $Q$  or large negative  $\Lambda$ . Many additional families bifurcate into existence in saddle-node bifurcations. Some of these are plotted twice in Figure 5.2(b), as they correspond to asymmetric solutions and their value at the center of either ring may be used as the input parameter  $q$  in the shooting function.

An alternative to a numerical shooting method is to use the fact that the solution on each edge is given by a cnoidal or dnoidal function, see Appendix A, or by a hyperbolic secant and use the boundary conditions (1.4b) and (1.4c), together with the complete ring assumption to derive nonlinear equations for the parameters in these solutions. This is the approach taken in reference [20].

### 5.3 Two complete rings

Solutions of this type can be completely described analytically, including the values at  $\Lambda$  for which they bifurcate. Doing so, however, is somewhat unwieldy, as there are many cases to consider. The restriction to each ring must be an integer number of periodic orbits of Equation (1.5), and on the restriction to central edge must be an integer number of half-period orbits, with  $\phi'_2(\pm L) = 0$ . One such solution is shown in Figure 5.3.

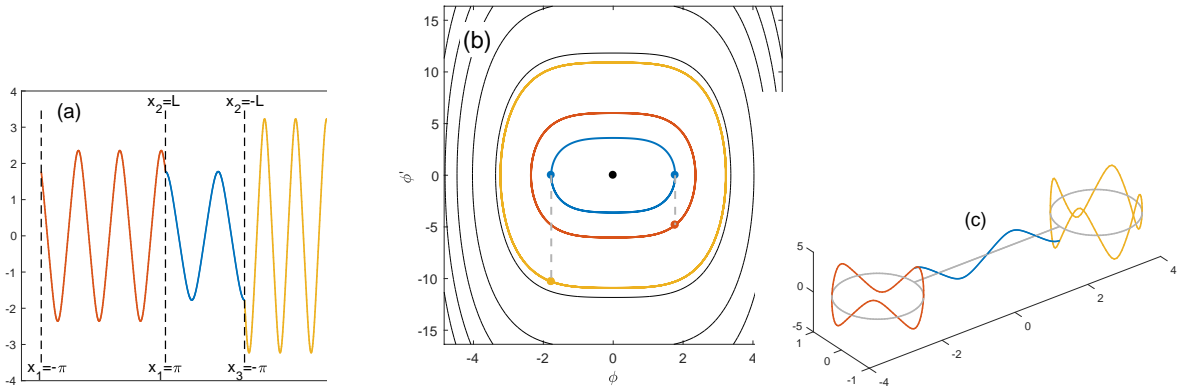


Figure 5.3: Three views of a typical solution with two complete rings.

We can classify all such solutions with a triple  $(n_1, m, n_3)$  as follows

- If  $n_i = 0$  or  $m = 0$  then the solution vanishes on the indicated edge.
- We use the label  $n_i = \Lambda$  or  $m = \Lambda$  if the  $\phi = \sqrt{\frac{-\Lambda}{2}}$  on the indicated edge. This can occur only for  $\Lambda < 0$ .
- $n_i > 0$  if the solution contains exactly  $n_i$  periods of the cn function on ring  $i$  and  $n_i < 0$  if the solution contains exactly  $|n_i|$  periods of the dn function on ring  $i$ . The former can only occur for  $\Lambda < n_i^2$ . and the latter for  $\Lambda < -n_i^2/2$ .

- $m > 0$  if the edge  $e_2$  contains exactly  $m$  half-periods of the cn function and  $m < 0$  if the central edge contains exactly  $|m|$  half-periods of the dn function. The former can occur only for  $\Lambda < m^2\Lambda^*$  and the latter for  $\Lambda < -m^2\Lambda^*/2$ , where  $\Lambda^* = \left(\frac{\pi}{2L}\right)^2$ .

Therefore, the trivial solution  $(0, 0, 0)$  exists for all  $\Lambda$ , and the other solutions emerge as  $\Lambda$  is decreased. We present a minimal list, and omit additional solutions obtained from group orbits of these solutions under (1.6).

- At  $\Lambda = n_1^2$ , the solutions  $(n_1, 0, n_1)$  and  $(n_1, 0, 0)$  bifurcate from  $(0, 0, 0)$ . Simultaneously, for all  $n_3 > n_1$ , the solution  $(n_1, 0, n_3)$  bifurcates from  $(0, 0, n_3)$ .
- At  $\Lambda = m^2\Lambda^*$ , the solution  $(n_1, m, n_3)$  bifurcates from  $(n_1, 0, n_3)$  if  $m < 2Ln_{1,3}/\pi$ .
- At  $\Lambda = 0$ , the solution  $(\Lambda, \Lambda, \Lambda)$  bifurcates from  $(0, 0, 0)$ . Simultaneously  $(n_1, \Lambda, n_3)$  from  $(n_1, 0, n_3)$  for all  $n_{1,3} \geq 0$ .
- At  $\Lambda = -m^2\Lambda^*/2$ , solutions of the form  $(n_1, -|m|, n_3)$  bifurcate from those of the form  $(n_1, \Lambda, n_3)$ . Note that if  $m < 0$  is odd and  $n_1 \neq n_3$  then  $(n_1, m, n_3)$  and  $(n_3, m, n_1)$  are not related by symmetry.
- at  $\Lambda = -n_1^2/2$ , solutions  $(-|n_1|, \Lambda, -|n_1|)$  and  $(-|n_1|, \Lambda, \Lambda)$  bifurcate from  $(\Lambda, \Lambda, \Lambda)$ . Simultaneously  $(-|n_1|, \Lambda, n_3)$  bifurcates from  $(\Lambda, \Lambda, n_3)$  for all  $n_3 > -|n_1|$ .

All the resulting branches are displayed in Figure 5.4. Solutions at the five indicated points on this bifurcation diagram are displayed in Figure 5.5

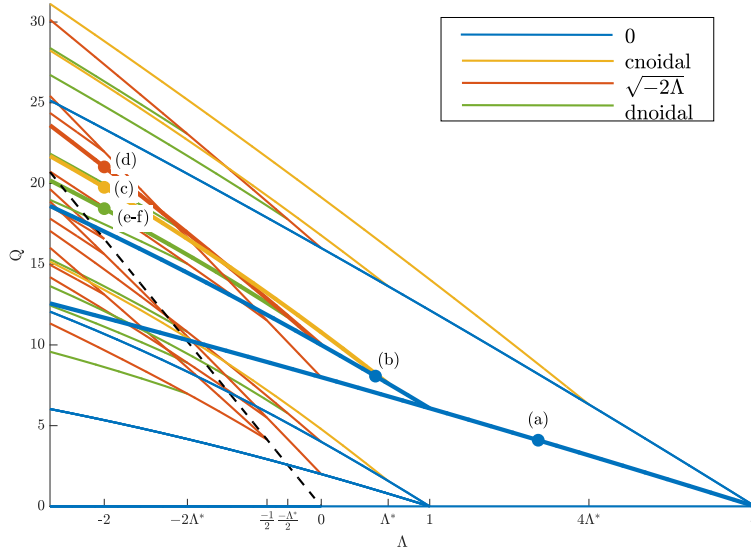


Figure 5.4: Bifurcation diagram for solutions with two complete rings. Plotted are solutions with  $|n_j| \leq 2$  and  $|m| \leq 2$ . Color indicates type of solution on the edge  $e_2$ . The dashed line shows the nonzero constant solution  $\Phi = \sqrt{-\Lambda/2}$ .

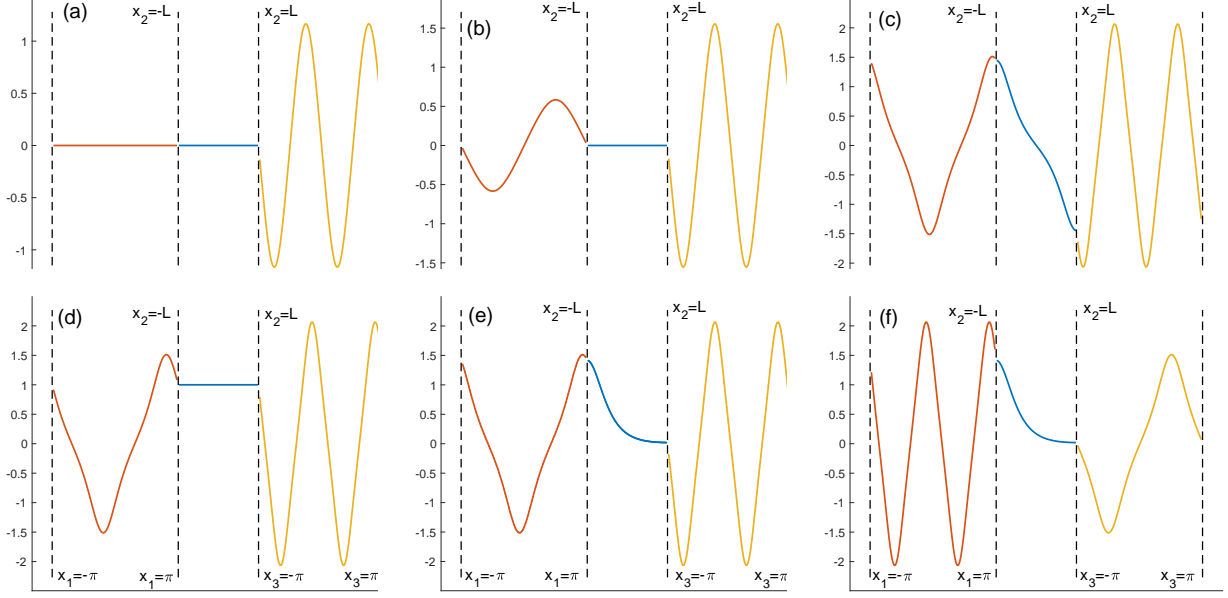


Figure 5.5: The standing waves at the six marked points in the bifurcation diagram of Figure 5.4. (a)  $(0, 0, 2)$ , (b)  $(1, 0, 2)$ , (c)  $(1, 1, 2)$ , (d)  $(1, \Lambda, 2)$ , (e)  $(1, -1, 2)$ , (f)  $(2, -1, 1)$ . Note from (e) and (f) that reversing  $n_1$  and  $n_3$  is not equivalent to a symmetry operation since a half-period of the  $dn$ -function has no symmetries. As  $\Lambda$  decreases, (b) bifurcates from (a), and then (c), (d), and (e-f) bifurcate from (b) in that order.

## 5.4 One incomplete and one complete ring

Solutions of this type have two parts. Assume that the incomplete ring lies on edge  $\mathbf{e}_1$ , then at vertex  $\mathbf{v}_2$ , we have  $\phi_2'(L) = 0$ . Therefore the solution on the lollipop-shaped subgraph formed by excluding  $\mathbf{e}_3$  is a nonlinear standing wave with Neumann boundary condition at vertex  $\mathbf{v}_2$ . We may find all such solutions by the same combination of shooting argument and numerical continuation described in Section 5.2. For a given value of  $\Lambda$ , this may be extended to a standing wave on the dumbbell graph if there exists a cnoidal solution of the form (A.1) with  $T = 2\pi/n$  and  $|\phi_2(L)| \leq \alpha$ , or if there exists a dnoidal solution of the form (A.3) with  $T = 2\pi/n$  and  $\sqrt{1 - k^2}a \leq |\phi_2(L)| < a$ .

Figure 5.6(a) shows, superimposed, the results of two computations. The solid curves show the solutions of the problem on the lollipop subgraph with Neumann condition at vertex  $\mathbf{v}_2$ . We have plotted  $\phi_2(\mathbf{v}_2)$  as a function of  $\Lambda$ . Also plotted are the maximum value of the cnoidal solutions quantized on the ring, for  $n = 1, 2$  and the minimum and maximum values of the dnoidal solutions quantized on the ring for  $n = 1, 2$ . Solutions on the lollipop can be extended to the dumbbell if  $|\phi_2(\mathbf{v}_2)|$  is below the maximum of the cnoidal function or between the minimum and the maximum of the dnoidal function. In addition to the bifurcations of the lollipop solutions, saddle-node bifurcations occur where the lollipop solution curves cross the curves of complete ring solutions.

A bifurcation diagram for these solutions on the dumbbell is shown in Figure 5.6(b). Note that none of the solutions bifurcate from  $Q = 0$ . Points where the curve appears to end are actually saddle-node bifurcations corresponding to the crossings described in the previous paragraph.

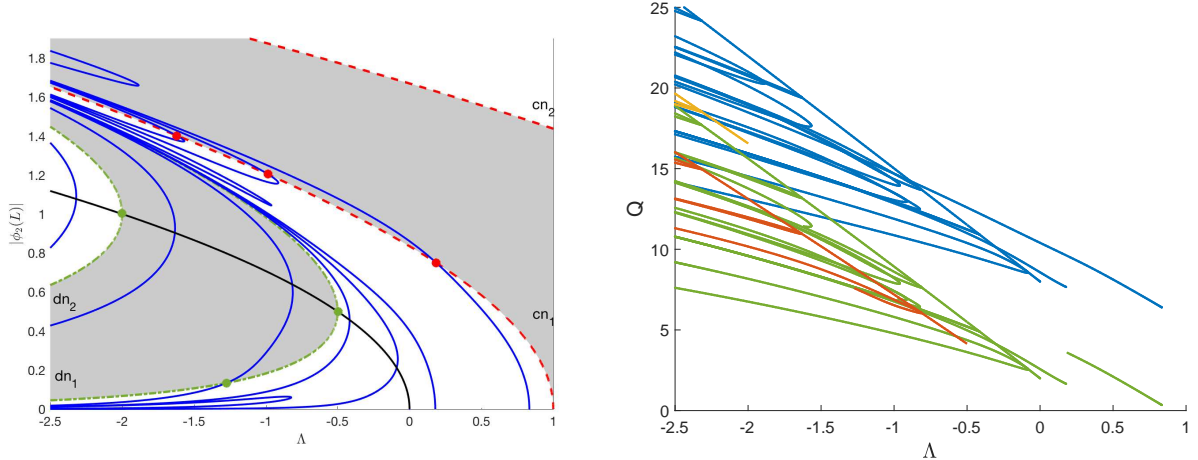


Figure 5.6: (a) Solid curves: Partial bifurcation diagram on the lollipop subgraph. Dashed curves indicate the maximum values of the quantized cnoidal solutions and the dash-dot the maximum and minimum values of the quantized conoidal solutions on edge  $e_3$ , with the regions between them shaded, alternately, for clarity. The marked points at intersections between the two families of curves indicate saddle node bifurcations of solutions with cnoidal or dnoidal solutions on the edge  $e_3$ . (b) Partial bifurcation diagram on the dumbbell graph.

## 6 Conclusion

To this author, the central question raised by Marzuola and Pelinovsky is whether the bifurcation scenario they see for NLS on the dumbbell graph is fundamentally different from that seen in other simpler systems. The far simpler bowtie DST system possesses the bifurcation structure identical to what they found, indicating that the phenomenon does not depend on the system being a quantum graph, but suggesting that the topology of the graph is important. This is confirmed by explicit comparison with the analogous problem posed on a line segment. The self-connected edges can be thought of as providing a singular perturbation to this simpler system, one which breaks the symmetry of half the families of solutions and thereby transforms pitchfork bifurcations into transcriticals. By contrast, the lollipop graph has less symmetry than the dumbbell and thus only transcriticals.

In the opposite direction, conceptually, we have shown how to enumerate the complete set of standing waves for this system, revealing a tremendous amount of complexity. Nonetheless, we have only been able to understand this much because of the relative simplicity of the dumbbell graph. In particular, the ring structure only permits two types of behavior at the vertices, and from this we are able to classify the solutions into three types. Further, the shooting methods described above depend strongly on the simple arrangement of the three edges. On a graph with many branches, or cycles, such shooting methods would be untenable.

We have not discussed stability of these standing waves as was done in [20], other than for the constant valued solution. Of special interest would be the stability of the solutions of the type  $(n_1, 0, n_3)$  discussed in Section 5.2. Because the phase of the solution is ill-defined on the edge  $e_2$ , the components on the other two edges can each be multiplied by an arbitrary phase. We may ask whether the stability depends on this phase. Beyond this, we can easily construct solutions which

vanish on  $\mathbf{e}_2$  and for which the solutions on the other two edges oscillate at different frequencies. Determining the stability of these solutions involves analyzing a genuinely time-dependent problem requiring Floquet theory.

Finally, In addition, recent work by Kirr has made progress toward analysis that identifies all the coherent states of a given nonlinear wave system using global bifurcation theory and perturbations from the large-amplitude limit [15]. It would be of interest to see if such an approach could be useful in studying the  $\Lambda \rightarrow -\infty$  limit of the standing wave problem.

## Acknowledgments

The author thanks Jeremy Marzuola and Dmitry Pelinovsky for many informative discussions and suggestions, and Stephen Shipman for reading and commenting on the manuscript. The author gratefully acknowledges the support of the Institute for Mathematics and its Applications (IMA) during the 2016–17 program in Mathematics and Optics, where this research was initiated.

## A Jacobi elliptic function solutions

This section provides formulas for exact solutions to Equation (1.5), it makes use of basic facts about elliptic integrals and Jacobi elliptic functions that can be found, for example, in Chapters 19 and 22 of [10].

For  $\Lambda > 0$ , the exact solutions are given by cnoidal functions,

$$\Phi = \alpha \operatorname{cn}(\beta x - \tau, \kappa), \quad (\text{A.1})$$

where

$$0 \leq \kappa < \frac{1}{\sqrt{2}}, \quad \alpha^2 = \frac{\kappa^2 \Lambda}{1 - 2\kappa^2}, \quad \text{and} \quad \beta^2 = \frac{\Lambda^2}{1 - 2\kappa^2}.$$

This has period

$$T_{\text{cn}} = 4K(\kappa) \sqrt{\frac{1 - 2\kappa^2}{\Lambda}}, \quad (\text{A.2})$$

where  $K(\kappa)$  is the complete elliptic integral of the first kind. As  $\kappa \rightarrow 0^+$ ,

$$T \rightarrow \frac{2\pi}{\sqrt{\Lambda}}$$

and the solution trajectories shrink to a point at the origin. As  $\kappa \rightarrow \frac{1}{\sqrt{2}}^-$ ,

$$T \rightarrow 0,$$

and the diameter of the trajectory diverges.

For  $\Lambda < 0$ , there are two types of periodic orbits. The first lie outside the separatrices shown in Figure 3.1 and are given by the same formulas as above, only for  $\frac{1}{\sqrt{2}} < \kappa < 1$ . As  $\kappa \rightarrow 1^-$ , these orbits approach the separatrices and their period diverges. As  $\kappa \rightarrow \frac{1}{\sqrt{2}}^+$ , the diameter of these orbits diverge, and their period approaches zero.

The other types of solution trajectories lie inside one or the other of the separatrices,

$$\Phi = \pm a \operatorname{dn}(bx - \tau, k), \quad (\text{A.3})$$

with

$$0 \leq k < 1, \text{ and } a = b = \sqrt{\frac{\Lambda}{k^2 - 2}}$$

and period

$$T_{\text{dn}} = 2K(k) \sqrt{\frac{k^2 - 2}{\Lambda}}. \quad (\text{A.4})$$

As  $k \rightarrow 0^+$ , these periodic orbits shrink toward the nonzero fixed points and

$$T \rightarrow \frac{\pi\sqrt{2}}{\sqrt{-\Lambda}}.$$

As  $k \rightarrow 1^-$ , these orbits approach the separatrices and their periods diverge.

## References

- [1] R. Adami, C. Cacciapuoti, D. Finco, and D. Noja. Stationary states of NLS on star graphs. *EPL–Europhys. Lett.*, 100:10003, 2012.
- [2] M. Arioli and M. Benzi. A Finite Element Method for Quantum Graphs. *IMA J. Numer. Anal.*, to appear, 2017.
- [3] G. Berkolaiko. An elementary introduction to quantum graphs. *ArXiv e-prints*, math:arXiv:1603.07356, 2016.
- [4] G. Berkolaiko and P. Kuchment. *Introduction to Quantum Graphs*. Mathematical surveys and monographs. American Mathematical Society, 2013.
- [5] J. Bolte and J. Kerner. Many-particle quantum graphs and Bose-Einstein condensation. *J. Math. Phys.*, 55:061901, 2014.
- [6] C. Cacciapuoti, D. Finco, and D. Noja. Topology-induced bifurcations for the nonlinear Schrödinger equation on the tadpole graph. *Phys. Rev. E*, 91:013206, 2015.
- [7] B. Delourme, S. Fliss, P. Joly, and E. Vasilevskaya. Trapped modes in thin and infinite ladder like domains. Part 1: Existence results. *Asymptotic Anal.*, 103:103–134, 2017.
- [8] A. Dhooge, W. Govaerts, and Y. A. Kuznetsov. MATCONT: a MATLAB package for numerical bifurcation analysis of ODEs. *ACM T. Math. Software*, 29:141–164, 2003.
- [9] A. Dhooge, W. Govaerts, Y. A. Kuznetsov, H. G. E. Meijer, and B. Sautois. New features of the software MatCont for bifurcation analysis of dynamical systems. *Math. Comp. Model. Dyn.*, 14:147–175, 2008.
- [10] *NIST Digital Library of Mathematical Functions*. <http://dlmf.nist.gov/>, Release 1.0.15 of 2017-06-01. F. W. J. Olver, A. B. Olde Daalhuis, D. W. Lozier, B. I. Schneider, R. F. Boisvert, C. W. Clark, B. R. Miller and B. V. Saunders, eds.

- [11] J. C. Eilbeck and M. Johansson. The discrete nonlinear Schrödinger equation—20 years on. In R. S. MacKay, L. Vázquez, and M. P. Zorzano, editors, *Proceedings Of The Third Conference On Localization And Energy Transfer In Nonlinear Systems*, pages 44–67, Madrid, 2003. World Scientific.
- [12] J. C. Eilbeck, P. S. Lomdahl, and A. C. Scott. The discrete self-trapping equation. *Phys. D*, 16:318–338, 1985.
- [13] D. D. Holm. *Geometric Mechanics Part I: Dynamics and Symmetry*. Imperial College Press, 2nd edition, 2011.
- [14] P. G. Kevrekidis. *The Discrete Nonlinear Schrödinger Equation: Mathematical Analysis, Numerical Computations and Physical Perspectives*, volume 232 of *Springer Tr. Mod. Phys.* Springer, Berlin Heidelberg, 2009.
- [15] E.-W. Kirr. Long time dynamics and coherent states in nonlinear wave equations. In R. Melnik, R. Makarov, and J. Belair, editors, *Recent Progress and Modern Challenges in Applied Mathematics, Modeling and Computational Science*, volume 79 of *Fields Inst. Commun.* Springer, 2017.
- [16] P. Kuchment and O. Post. On the spectra of carbon nano-structures. *Communications in Mathematical Physics*, 275:805–826, 2007.
- [17] J. L. Marzuola and D. E. Pelinovsky. Ground State on the Dumbbell Graph. *Appl. Math. Res. Express*, 2016:98–145, 2016.
- [18] A. Nayfeh and B. Balachandran. *Applied Nonlinear Dynamics: Analytical, Computational and Experimental Methods*. Wiley Series in Nonlinear Science. Wiley, 2008.
- [19] H. Niikuni. Schrödinger operators on a periodically broken zigzag carbon nanotube. *P. Indian Acad. Sci.—Math. Sci.*, 127:471–516, 2017.
- [20] D. Noja, D. E. Pelinovsky, and G. Shaikhova. Bifurcations and stability of standing waves in the nonlinear Schrödinger equation on the tadpole graph. *Nonlinearity*, 28:2343–2378, 2015.
- [21] D. Noja, S. Rolando, and S. Secchi. Standing waves for the NLS on the double-bridge graph and a rational-irrational dichotomy. *ArXiv e-prints*, math:arXiv:1706.09616, 2017.
- [22] D. E. Pelinovsky and G. Schneider. Bifurcations of Standing Localized Waves on Periodic Graphs. *Ann. Henri Poincaré*, 18:1185–1211, 2016.
- [23] J. Yang. Stability switching at transcritical bifurcations of solitary waves in generalized nonlinear Schrödinger equations. *Phys. Lett. A*, 377:866–870, 2013.